DØ Note 5728-CONF

Search for MSSM Higgs Boson Production in the Decay $h \to \tau_\mu \tau_{had}$ with the DØ Detector at $\sqrt{s} = 1.96$ TeV

The DØ Collaboration
URL http://www-d0.fnal.gov
(Dated: July 25, 2008)

A search for the production of neutral Higgs bosons decaying into $\tau^+\tau^-$ final states is presented. One of the two τ leptons is required to decay into a muon while the other decays hadronically. The integrated luminosity is about 1.2 fb^{-1}, collected by the DØ Experiment at the Fermilab Tevatron collider during Run IIb.

Preliminary Results for Summer 2008 Conferences

I. INTRODUCTION

Neutral Higgs bosons produced in $p\overline{p}$ collisions at the Tevatron can decay into $\tau^+\tau^-$ final states. The cross section times branching fraction of the $h \to \tau^+\tau^-$ final state in the Standard Model (SM) is too small to play any role in the SM Higgs boson searches due to the large irreducible background from Drell-Yan production in the interesting (low mass) region. This, however, is different in the Minimal Supersymmetric Standard Model (MSSM), which predicts two Higgs doublets leading to five Higgs bosons: a pair of charged Higgs boson ($H^{\pm}$); two neutral CP-even Higgs bosons (h,H) and a CP-odd Higgs boson (A). At tree level, the Higgs sector of the MSSM is fully described by two parameters, which are chosen to be the mass of the CP-odd Higgs boson, m_A, and $\tan\beta$, the ratio of the vacuum expectation values of the two Higgs doublets. The Higgs boson production cross section is enhanced in the region of low m_A and high $\tan\beta$ due to the increased Higgs boson coupling to down-type quarks [1]. In addition, two of the three neutral Higgs bosons, commonly denoted by ϕ, are often nearly degenerate in mass, leading to a further increase in the cross section. In the low m_A, high $\tan\beta$ region of the parameter space, Tevatron searches can therefore probe several MSSM benchmark scenarios extending the search regions covered by LEP [2].

Inclusive searches for ϕ $(= H, h, A) \to \tau\tau$ have been performed with integrated luminosities of $\mathcal{L} = 1.0$ fb^{-1} by DØ [3] in Run IIa and $\mathcal{L} = 1.8$ fb^{-1} by CDF [4] in Run IIa and IIb. These searches require the tau lepton pairs to decay into three final states: $\tau_e\tau_{had}$, $\tau_\mu\tau_{had}$, and $\tau_e\tau_\mu$, where τ_e and τ_μ are the leptonic decay of the tau and τ_{had} is the hadronic decay mode. In this note, the decay $\phi \to \tau_\mu\tau_{had}$ is considered using the DØ Run IIb data set with an integrated luminosity of $\mathcal{L} = 1.2$ fb^{-1}. The search strategy relies primarily on implementing an efficient tau identification algorithm in conjunction with a series of selections that remove backgrounds, which are dominated by electroweak $Z/\gamma^* \to \tau\tau$ and $Z/\gamma^* \to \mu\mu$ processes as well as those from heavy-flavor multijet events where a jet can be misidentified as a τ candidate.

II. DATASET AND MONTE CARLO SAMPLES

The analysis presented here is based on data collected between June 2006 and August 2007 by the DØ detector at the Fermilab Tevatron Collider. Events must fire at least one of the nine available single muon triggers. Data quality definitions are applied to remove all runs marked as 'bad' by each subdector's quality requirements.

The majority of background Monte Carlo events used in the analysis are generated with PYTHIA version 6.413 [5] and are then processed with GEANT, which provides a full simulation of the detector. Subsequently, the same reconstruction procedure as is used for the data is applied to Monte Carlo events. With the exception of QCD multijet and W boson production, the diboson and $t\bar{t}$ background processes are normalized using cross sections calculated at next-to-leading order (NLO) while for Z/γ^* production, those at next-to-NLO (NNLO) are used [6]. Duplicate events and events originating from a bad run are removed prior to normalization.

III. EVENT PRESELECTION

The preselection requires one isolated μ and one hadronic τ candidate. Muons with transverse momentum $p_{\rm T} > 10$ GeV are selected using patterns of hits in the muon detector matched to tracks in the central tracking detector. The muon must lie within $|\eta| < 2.0$, where η is the pseudorapidity defined by the muon detector system, so that the inclusive muon trigger requirements are fulfilled. The distance along the z direction, Δz, between the muon track and the primary vertex must be less than 1 cm.

Hadronically decaying taus characterized by a narrow isolated jet are classified into three types, which are distinguished by their detector signatures as follows:

- **Type 1:** Calorimeter cluster, with one associated track and no EM subcluster. This corresponds mainly to the decay $\tau^{\pm} \to \pi^{\pm}\nu$ ($\pi\nu$-like).
- **Type 2:** Calorimeter cluster, with one associated track and at least one EM subcluster. This corresponds mainly to the decay $\tau^{\pm} \to \pi^{\pm}\pi^0\nu$ ($\rho\nu$-like).
- **Type 3:** Calorimeter cluster, with two or three associated tracks, with or without EM subclusters. This corresponds mainly to the decays $\tau^{\pm} \to \pi^{\pm}\pi^{\pm}\pi^{\mp}(\pi^0)\nu$ (3-prong).

An event is required to contain a τ candidate at a distance $\Delta R_{\mu\tau} = \sqrt{(\Delta\phi)^2 + (\Delta\eta)^2} > 0.5$, from the muon direction and with a charge opposite to the muon charge. The transverse momentum of the τ candidate, p_T^τ, must be greater than 15 GeV for τ-types 1 and 2, and greater than 20 GeV for τ-type 3. Further, the transverse momentum of the

track associated with the τ candidate is required to be $p_T > 15$ GeV for τ-type 1 and $p_T > 5$ GeV for τ-type 2. In the case of τ-type 3, one of the associated tracks must have $p_T > 5$ GeV and the scalar sum of the transverse momenta of all associated tracks must be greater than 15 GeV. At least one of the tau tracks must have a minimum of one SMT hit (this requirement is for all tau types). The distances Δz, where the positive z-axis is along the proton beam direction, between a) the τ and the primary vertex and b) the τ and the muon track must both be less than 1 cm. An energy correction for taus, derived from data based on the ratio of the calorimeter energy with track p_T, is applied on the prediction (MC) to better match the tau energy spectrum in data. A τ Neural Network (NN_τ) is applied at a later stage in the analysis to separate real taus from those that originate from jet fakes. A separate NN_τ has been trained for each tau type.

Jets are calibrated using the standard DØ Jet Energy Scale (JES) measurement [7]. The missing energy is corrected for the selected muon and any jet of $p_T^{JES} > 20$ GeV, where p_T^{JES} is the JES corrected transverse momentum of the jet. Jets that match tau candidates passing the above requirements and have $NN_\tau > 0.8$ are not used in the missing energy correction. This avoids using the JES corrections on real tau candidates. Events are required to have no electrons with $p_T > 12$ GeV. This ensures this analysis is orthogonal to the $e\mu$ channel.

After preselections, the data sample is expected to be dominated by W events in association with a jet (W+jets) and QCD background. Here, the primary contributions are from multi-jet events, particularly those with heavy flavor events, where a muon from a semi-leptonic decay passes the isolation requirement and a jet is misidentified as a τ. In addition, a contribution is expected from light quark multi-jet events where the jets fake both the tau and the muon. This background source is difficult to simulate, and therefore, is estimated using data. In particular, the NN_τ distribution is used by determining the number of events with intermediate NN_τ values, which are expected to be dominated mainly by contributions from QCD+W. The total number of events is then extrapolated to higher values of NN_τ where signal-like events containing a tau are predicted. Figure 1 shows the muon p_T with the shape estimated for QCD+W.

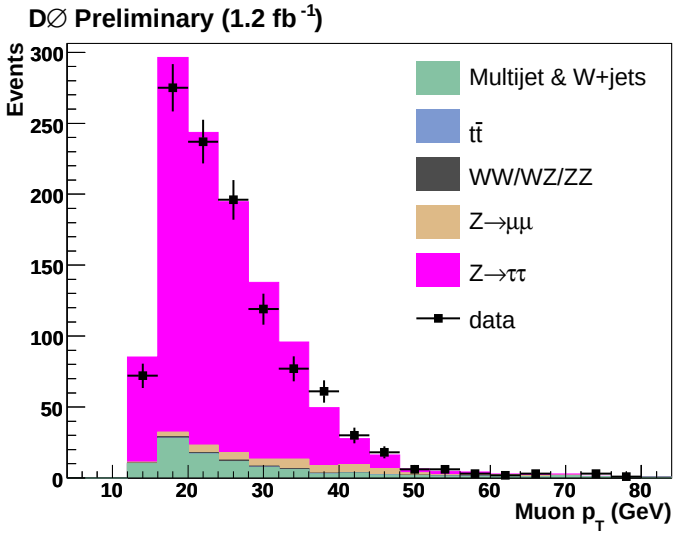

FIG. 1: Muon transverse momentum for the data, shown with error bars, compared to the sum of the expected backgrounds with the QCD shape estimated from data. Only statistical uncertainties on the data are shown.

IV. FINAL SELECTION

A series of selections is used to further reduce the backgrounds from $Z \to \mu\mu$, W+jets and QCD. At this stage no attempt is made to remove contribution from $Z/\gamma^* \to \tau\tau$, since it is irreducible except for the differences in mass and spin, *i.e.,* angular distribution with respect to the Higgs boson.

1. NN_τ is applied to discriminate taus from jets. Here, NN_τ is required to be greater than 0.9 for τ-types 1 and 2, and greater than 0.95 for τ-type 3. The selection is kept tighter for τ-type 3 due to the larger QCD and W+jets backgrounds.

2. Events where τ candidates are matched to a loose, central muon within $\Delta R_{\mu\tau} < 0.5$, where no $p_{\rm T}$ cut is applied to the muon, are rejected. This removes much of the remaining $Z \to \mu\mu$ background.

3. During preselections, muons with $p_T > 10$ GeV and -2.0 $< |\eta| <$ 2.0 were selected. However, due to constraints imposed by the Level 1 (L1) single muon triggers, this requirement is adjusted by raising the minimum muon p_T to 15 GeV and -1.6 $< |\eta| <$ 1.6.

4. Select events with the transverse mass, M_T, defined by:

$$M_T = \sqrt{2 p_T^{\mu} \not{E}_T (1 - \cos\Delta\phi)} \tag{1}$$

In particular, require M_T between the μ-τ pair to be less than 40 GeV. This selection removes most of the W+jets background.

V. COMPARISONS OF DATA WITH EXPECTED BACKGROUND

Table I lists the yields from data compared to the expected backgrounds for each of the three tau types and the sum of all types, respectively. Further, Fig. 2 provides the p_T^{τ} distribution for the tau candidates after the transverse mass cut. Figure 3 provides the tau track p_T distribution for the tau candidates, where the scalar sum of track momenta for type 3 taus is used, after the transverse mass cut. Within statistics, the predicted backgrounds are consistent with the number of events in data for τ-types 1 and 2. For τ-type 3, the apparent discrepancy between the number of observed and predicted events is 1.5σ after incorporating the systematic uncertainties discussed in Sec. VI.

TABLE I: Prediction from MC and QCD backgrounds compared to the observation in data for each tau type and sum of all types. Only statistical errors on the MC and QCD are given.

τ-type	Data	$Z \to \tau\tau$	$Z \to \mu\mu$	QCD+W+jets	$WW/WZ/ZZ$	$t\bar{t}$	Predicted
1	162	129 ± 11	6 ± 2	22 ± 4	1 ± 1	0.3 ± 0.6	159 ± 12
2	709	655 ± 25	35 ± 5	45 ± 6	4 ± 2	1.5 ± 1.2	741 ± 27
3	238	251 ± 15	6 ± 2	33 ± 5	1 ± 1	0.8 ± 0.9	293 ± 17
all types	1109	1030 ± 32	48 ± 6	96 ± 9	6 ± 2	2.7 ± 1.6	1189 ± 34

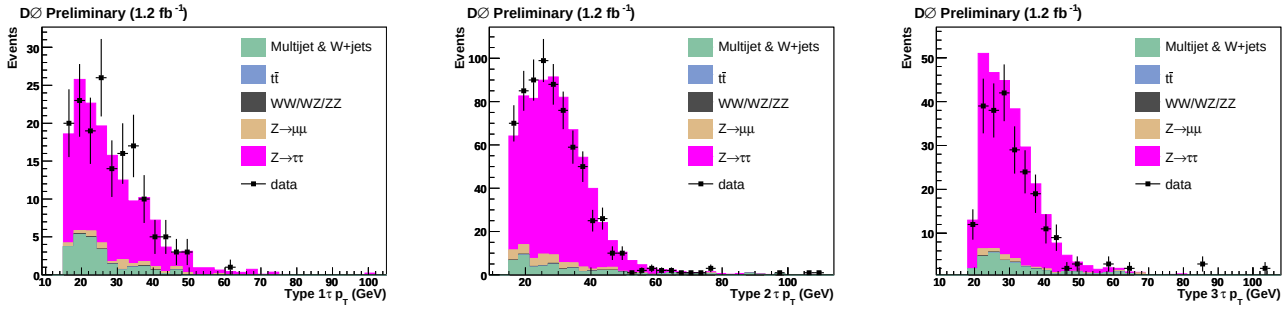

(a) (b) (c)

FIG. 2: Distribution of tau $p_{\rm T}$ for data, shown with error bars, compared to the sum of the expected backgrounds for τ-types 1 (a), 2 (b), and 3 (c) each after the transverse mass cut. Only statistical uncertainties on the data are shown.

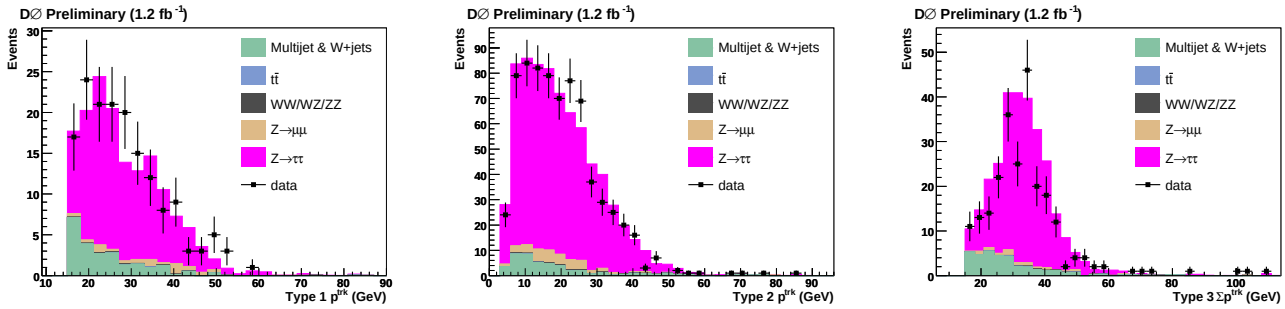

(a) (b) (c)

FIG. 3: Distribution of tau track p_{T} for data, shown with error bars, compared to the sum of the expected backgrounds for τ-types 1 (a), 2 (b), and 3 (c) each after the transverse mass cut. For τ-type 3, the scalar sum of the transverse momentum of the three tracks is used. Only statistical uncertainties on the data are shown.

VI. SYSTEMATIC UNCERTAINTIES

Various sources of systematic error affect both the signal efficiency and background estimations. The systematics from each source are summarized in Table II.

The uncertainty on the luminosity (6.1%), muon ID (4%), muon track (2%) and tau track (1.4%) efficiencies are all taken into account. The uncertainty on the Z cross section is taken to be 5% [6], to allow for scale and parton distribution function (PDF) uncertainties. The uncertainty on the trigger efficiency (5%) is estimated by varying the trigger probabilities of the single muon triggers by $\pm 1\sigma$. The error on the signal acceptance due to PDF uncertainties was estimated by comparing the acceptance of the signal when the MC is reweighted to the 20 available error sets in the CTEQ6.1 PDF, where each set contains the $\pm 1\sigma$ variations, and then adding the systematic uncertainties obtained from each in quadrature.

Systematics for the tau energy scale is assigned to be $2.7-3.6\%$ depending on τ-type and includes the 2% uncertainty on the JES. The uncertainty on the overall tau ID efficiency was estimated by comparing the fraction of events in each tau type between data and prediction. The predicted fraction for a given tau type i, is $f_i^{Pred} = n_i^{Pred}/n_{tot}^{Pred}$, where n_i^{Pred} is the number of events predicted for tau type i, and n_{tot}^{Pred} is the total number of events predicted. Similarly, the observed fraction in the data for a given tau type i, is $f_i^{Data} = n_i^{Data}/n_{tot}^{Data}$, where n_i^{Data} is the number of events in data for tau type i, and n_{tot}^{Data} is the total number of events in the data. Since the main systematics, which include the luminosity, trigger efficiency and the uncertainty on the Z cross section, are expected to be correlated between all three tau types, any difference in the fractions between data and prediction can be approximately taken to be due to uncertainties in the tau ID. This is only true in the final event sample where the purity of the $Z \to \tau\tau$ events is high. The difference between the predicted fraction for a given tau type i, $\Delta f_i = (f_i^{Pred} - f_i^{Data})/f_i^{Pred}$, is 8%, 4%, and 5% for τ-types 1, 2, and 3, respectively. These numbers are used as the uncertainty estimate on the tau ID efficiency. Such systematics are also assumed to apply for the signal.

VII. FINAL RESULTS

The visible mass, M_{vis}, variable is used to search for the signal in the data sample. For τ-type 1, which by definition contain charged single pion decays, the track momentum is used as the momentum for the tau as it provides a better measurement for the visible mass. On the other hand, for τ-types 2 and 3, where a contribution from neutral pions can exist, the calorimeter momentum is used. The variable is defined as:

$$M_{\mathrm{vis}} = \sqrt{(P_{\tau_1} + P_{\tau_2} + \not{P}_{\mathrm{T}})^2}, \tag{2}$$

and is calculated using the four vectors of the visible tau decay products $P_{\tau_{1,2}}$ and of the missing momentum $\not{P}_{\mathrm{T}} = (\not{E}_T, \not{E}_{\mathrm{x}}, \not{E}_{\mathrm{y}}, 0)$. $\not{E}_{\mathrm{x}}$ and $\not{E}_{\mathrm{y}}$ indicate the components of $\not{E}_T$. The visible mass for events passing the final selection is shown in Fig. 4 for a Higgs boson mass of 160 GeV. Similar distributions are also studied at different Higgs

TABLE II: Summary of the various sources of systematic error for both the signal and background.

Source of Systematic Error	Relative Error on	
	B ackground	Signal
Luminosity	6.1%	6.1%
Muon Track Match	2%	2%
Muon ID	4%	4%
Tau Track Match	1.4%	1.4%
Tau ID (depend on τ-type)	$4-8\%$	$4-8\%$
Trigger	5%	5%
Tau Energy Scale (depend on τ-type)	$2.7-3.6\%$	$2.7-3.6\%$
QCD	3.2%	—
$Z/\gamma^* \rightarrow ll$ cross section	5%	—
PDF variation	—	4.6%

masses within the range of 90 to 300 GeV. Since no significant excess in signal over background is observed, limits on the production cross section times branching fraction for neutral Higgs boson decaying to tau pairs is calculated. Specifically, the visible mass variable is used as the input to the limit calculator `collie` [9]. The limit is calculated using the CL_s method applying the Gaussian smearing of the systematics (CLsyst). Figures 5 and 6 show the expected and observed cross section limits and the log-likelihood ratio (LLR) with $\pm 1\sigma$ and $\pm 2\sigma$ bands of Gaussian systematics compared to the DØ Run IIa expected limit.

The above discussion includes limits on the cross section times branching fraction for neutral Higgs boson decaying to tau pairs in Run IIb and subsequently, these can be combined with the DØ Run IIa result, for a total integrated luminosity of 2.2 fb^{-1}. The results can further be interpreted in the Minimal Supersymmetric Standard Model (MSSM). These results are fully described in a separate note [10].

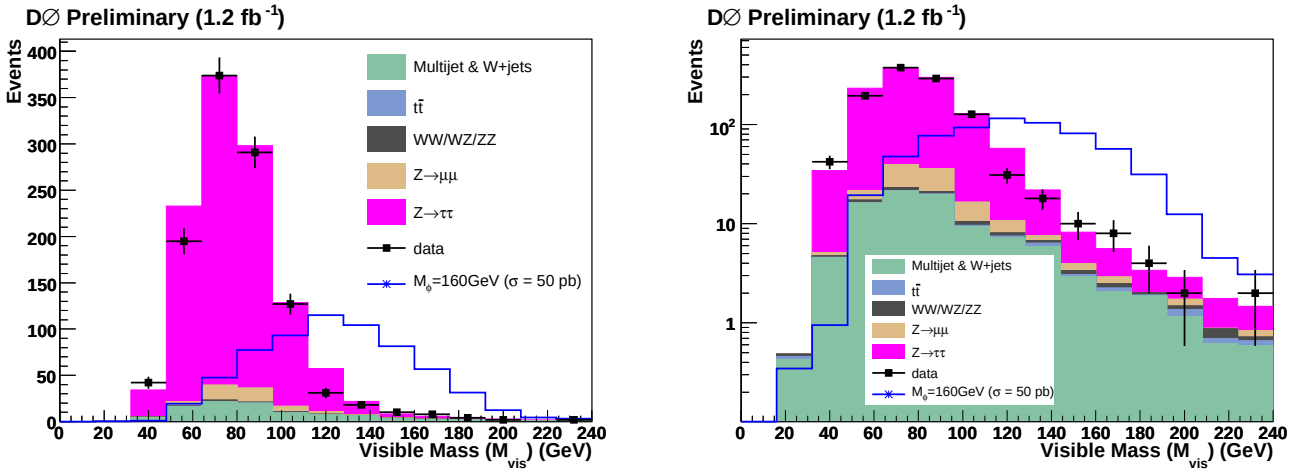

(a) (b)

FIG. 4: Distribution of the visible mass, $M_{\rm vis}$, after all selections applied on (a) a linear scale and (b) a log scale. The data, shown with error bars, is compared to the sum of the expected backgrounds. Also shown, in blue open histogram, is the signal for a Higgs mass of 160 GeV assuming a signal cross section times branching fraction of 50 pb.

Acknowledgments

We thank the staffs at Fermilab and collaborating institutions, and acknowledge support from the DOE and NSF (USA); CEA and CNRS/IN2P3 (France); FASI, Rosatom and RFBR (Russia); CNPq, FAPERJ, FAPESP and

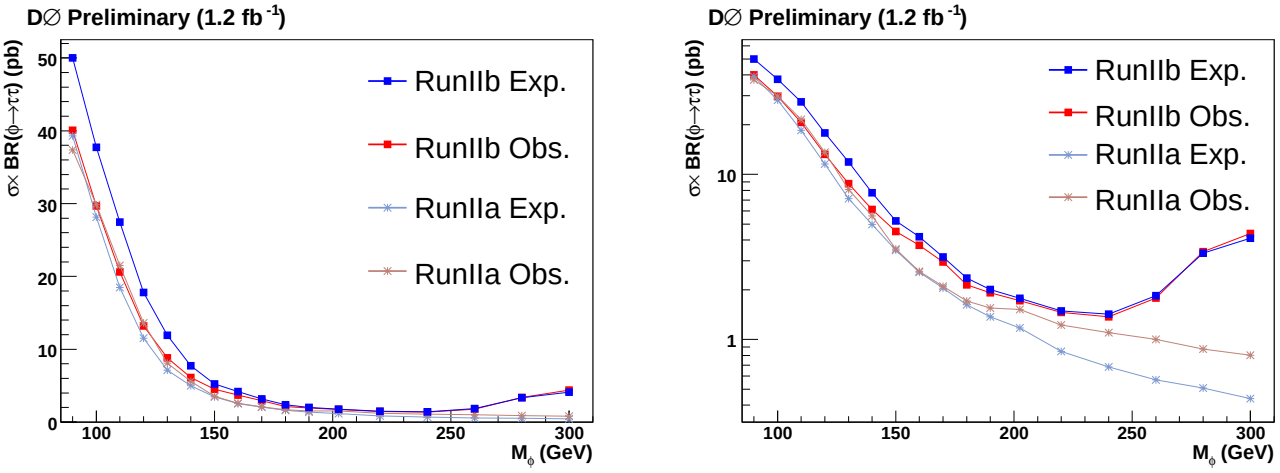

(a) (b)

FIG. 5: Expected and observed upper limits on the cross section times branching ratio for $\phi \rightarrow \tau_\mu \tau_{had}$ production as a function of m_ϕ assuming the SM width of the Higgs boson on (a) a linear scale and (b) a log scale.

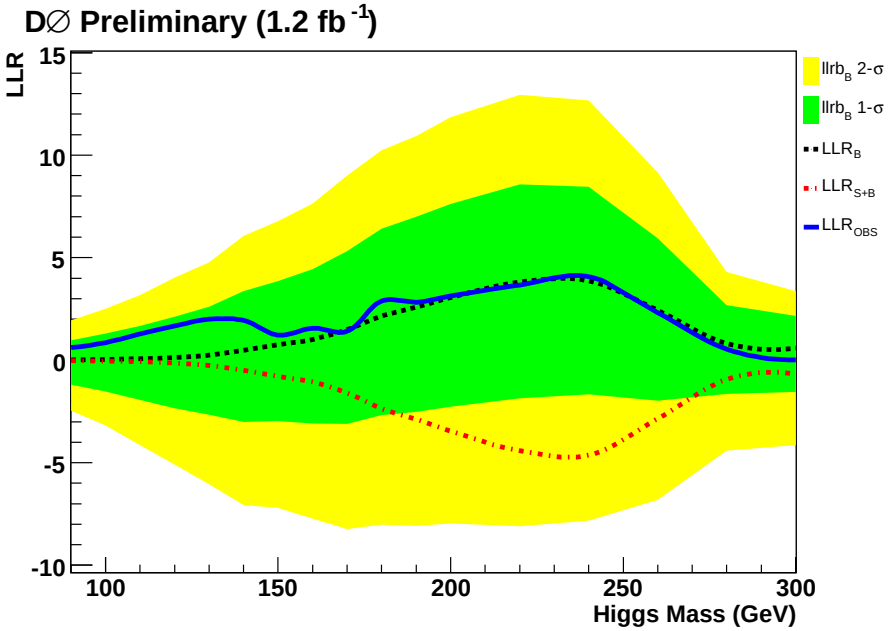

FIG. 6: Log-Likelihood Ratio (LLR) as a function of Higgs boson mass with $\pm 1\sigma$ (green) and $\pm 2\sigma$ (yellow) bands of the Gaussian systematics. Shown by the solid blue curve is the observed result.

FUNDUNESP (Brazil); DAE and DST (India); Colciencias (Colombia); CONACyT (Mexico); KRF and KOSEF (Korea); CONICET and UBACyT (Argentina); FOM (The Netherlands); STFC (United Kingdom); MSMT and GACR (Czech Republic); CRC Program, CFI, NSERC and WestGrid Project (Canada); BMBF and DFG (Germany); SFI (Ireland); The Swedish Research Council (Sweden); CAS and CNSF (China); and the Alexander von Humboldt

Foundation (Germany).

---

[1] M. Carena, S. Heinemeyer, C.E.M Wagner and G. Weiglein, Eur. Phys. J. C. **45** 797 (2006).
[2] The ALEPH, DELPHI, L3 and OPAL Collaborations, S. Schael *et al.*, Eur. Phys. J. C. **47** 547 (2006).
[3] DØ Collaboration, FERMILAB-PUB-08/132-E, Accepted by PRL (2008).
[4] CDF Collaboration, October 2007, URL:
`http://www-cdf.fnal.gov/physics/new/hdg/results/htt_070928`
[5] T. Sjöstrand *et al.*, Comput. Phys. Commun. **135**, 238 (2001).
[6] T. Nunnemann, June 2004, URL: `http://www-clued0.fnal.gov/ nunne/cross-sections/nnlo_xsect.html`
[7] V. M. Abazov *et al.*, (D0 Collaboration), FERMILAB-PUB-08/034-E (2008).
[8] S. Heinemeyer, W. Hollik, G. Weiglein, Comput. Phys. Comm. 124, 76 (2000).
[9] W. Fisher, FERMILAB-TM-2386-E (2007).
[10] DØ Collaboration, D0 Note 5740-CONF.